


Induced-Photorefractive Attack against Quantum Key Distribution

Peng Ye^{1,2}, Wei Chen^{1,2,*}, Guo-Wei Zhang^{1,2}, Feng-Yu Lu^{1,2}, Fang-Xiang Wang^{1,2}, Guan-Zhong Huang^{1,2}, Shuang Wang^{1,2}, De-Yong He^{1,2}, Zhen-Qiang Yin^{1,2}, Guang-Can Guo^{1,2} and Zheng-Fu Han^{1,2}

¹*CAS Key Laboratory of Quantum Information, University of Science and Technology of China, Hefei 230026, China*

²*CAS Center for Excellence in Quantum Information and Quantum Physics, University of Science and Technology of China, Hefei 230026, China*

 (Received 14 July 2022; revised 17 February 2023; accepted 12 April 2023; published 16 May 2023)

Lithium niobate (LiNbO₃, LN) devices play critical roles in quantum information processing. However, for special applications like quantum key distribution (QKD), the characteristics of materials and devices and their impact on practical systems must be intensively explored. For the first time, we reveal that the photorefractive effect in LN can be utilized as a potential loophole to carry out malicious attacks by the eavesdroppers. We take a commercial LN-based variable optical attenuator as an example to demonstrate the method we name the induced-photorefractive attack (IPA) and propose two techniques to enable controllable attacks. Our results show that eavesdroppers can fulfill an efficient source-side attack by injecting an optimized irradiation beam with only several nanowatts, which is realistic when accessing commercial fiber channels. These measures and techniques can be employed for all individual and on-chip LN devices. Our work opens a new window for the security research of real-life QKD and contributes to designing QKD systems with higher security.

DOI: [10.1103/PhysRevApplied.19.054052](https://doi.org/10.1103/PhysRevApplied.19.054052)

I. INTRODUCTION

The photoinduced index change procedure in lithium niobate (LN) is known as the photorefractive effect (PE), which causes a phase shift between the illuminating profile and the index pattern [1]. As an inherent property of LN [2], PE can remarkably change the index of the LN waveguide, which further influences a series of modulation results such as phase, intensity, polarization, or the extinction ratio [3,4] according to different device structures, making them no longer reliable. Although many studies have been conducted on the imperfections of LN devices [5,6], in-depth research on the security problems associated with the index change of a material has not been carried out from the perspective of practical security in quantum key distribution (QKD) systems.

For the first time, we propose that PE can be utilized by eavesdroppers (Eve) to actively modify the parameters of QKD systems and manipulate the results of quantum state preparation, which, at worst, may result in totally broken security. We analyze the mechanism of PE and the effect of the induced-photorefractive attack (IPA). We remark that PE is a new mechanism to cause loopholes and can be applied to affect almost all LN devices, such as intensity modulators, phase modulators, polarization

controllers, variable optical attenuators (VOAs), and choppers since PE is an inherent property of LN material. The implementation methods of attacks may differ for different types of LN devices. Here, a LN-based VOA in QKD transmitters is used as an example to verify IPA and two techniques are proposed to enable precisely controlled attacks. Simulation results show that Eve can completely steal the secure key without being perceived if she can control the attenuation of VOA. The experiment demonstrates that Eve can commit private hacking with just 3-nW irradiation power, which is 9 orders of magnitude lower than the laser-damage scheme [7]. This indicates that IPA can be executed from the available accessing points in real-life fiber channels.

In addition to fiber devices, PE is also present and more evident in chip-based LN devices owing to the stronger confinement of the optical mode in lithium-niobate-on-insulator (LNOI) waveguides [8–10]. As we know, LNOI-based high-speed modulators not only have a higher modulation bandwidth [11,12] but also do not have modulation-dependent loss [13,14] thanks to the Pockels effect [15]. It matches the requirements of QKD very well in terms of both the modulation and security. We believe that LNOI has great potential and application prospects in integrated QKD in the future; thus, PE-related issues should not be ignored. According to our results, the presence of PE should be seriously considered when designing

*weich@ustc.edu.cn

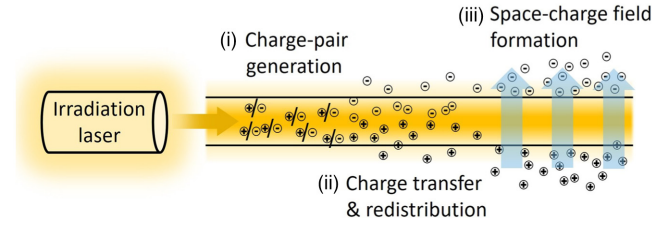


FIG. 1. Schematic diagram of the PE procedure.

QKD systems, and this work can give essential inspiration to enhance their practical security.

II. THE MECHANISM OF IPA

As shown in Fig. 1, the PE procedure can be described in three stages.

(i) *Charge-pair generation*: the irradiation beam excites photogenerated charge pairs from impurities and defect centers.

(ii) *Charge transfer and redistribution*: the charges are driven by the carrier concentration distribution, the electric field, or the photovoltaic effect; thus, they move out of the waveguide and get trapped in dark areas.

(iii) *Space-charge field formation*: the inhomogeneous charge distribution causes a space-charge field, which modulates the index of LN waveguides through the Pockels effect [16].

Under irradiation power I_{ir} , the photoinduced index change can be derived from the Kukhtarev equation [17]:

$$\Delta n(I_{\text{ir}}, t) = \frac{n^3 r_{33} \gamma}{2} E_s(I_{\text{ir}}, t) = \Delta n_s(I_{\text{ir}})(1 - e^{-t/\tau}). \quad (1)$$

Here $E_s(I_{\text{ir}}, t)$ is the space-charge field induced by PE; n is the waveguide refractive index at the signal wavelength; r_{33} is the Pockels coefficient; γ is the overlap integral of the optical mode profile and E_s ; and τ is the build-up time constant [18], which determines the response speed of PE and can be expressed as $\tau = \epsilon_r \epsilon_0 / (\sigma_d + \sigma_{\text{ph}})$, where ϵ_r and ϵ_0 are the relative and vacuum dielectric constants, respectively, σ_d is the dark conductivity, and σ_{ph} is the photoconductivity positively correlated with I_{ir} . The saturated photorefractive index change $\Delta n_s(I_{\text{ir}})$ is [19]

$$\Delta n_s(I_{\text{ir}}) = \frac{n^3 r_{33} \gamma}{2} \left(-\frac{\sigma_{\text{ph}}}{\sigma} E_{\text{app}} + \frac{\kappa \alpha}{\sigma} I_{\text{ir}} \right), \quad (2)$$

where E_{app} is the applied electric field, α is the absorption coefficient of the donor or acceptor centers, $\sigma = \sigma_d + \sigma_{\text{ph}}$, and κ is the Glass constant. See Appendix A for more details about PE.

As mentioned above, this index change causes the signal phase to change by $\theta_{\text{PE}} = 2\pi \Delta n_s L_{\text{eff}} / \lambda_0$, where L_{eff} is

the effective interaction length and λ_0 is the wavelength of signal photons, and then a series of modulation deviations in LN devices for signal photons. For example, the signal quantum state passing through a Mach-Zehnder interferometer (MZI) is

$$|\sqrt{\mu}\rangle = |i\sqrt{r(1-r)}(e^{i\Delta\theta} + 1)\sqrt{\mu_{\text{in}}}\rangle, \quad (3)$$

where μ_{in} is the mean photon number (MPN) of the input signal pulses, r is the beam-splitting ratio (BSR) of two beam splitters (BSs) in a MZI. The phase difference between the two arms is expressed as $\Delta\theta = \theta_{\text{arm1}} - \theta_{\text{arm2}}$. We can see that the index change of the LN waveguide under IPA influences both r and $\Delta\theta$ and then the signal quantum state $|\sqrt{\mu}\rangle$.

Some researchers consider that PE in a MZI only comes from the change of r because the PE on each arm can cancel each other [4]. But, in fact, since the fabrication error and the applied modulation electric fields E_{app}^j ($j = 1$ for the upper arm and $j = 2$ for the lower arm) are both different for the two arms of a MZI, their working conditions are not identical. Additionally, the I_{ir}^j in these two arms are also different because r deviated from 0.5 at the irradiation wavelength. According to Eq. (2), the differences in both E_{app}^j and I_{ir}^j on each arm leads to the inconsistent PE so that they cannot cancel each other. In contrast, the effect of r caused by PE is almost negligible at low irradiation power ($I_{\text{ir}} < 100$ mW) [16]. Hence we conclude that $\Delta\theta$ dominates the attenuation change.

The phase difference $\Delta\theta$ can be divided into three parts [19,20], which can be described as

$$\Delta\theta = \Delta\theta_0 + \Delta\theta_E + \Delta\theta_{\text{PE}}, \quad (4)$$

including a geometrical phase $\Delta\theta_0$, an electro-optic phase $\Delta\theta_E$, and a PE phase $\Delta\theta_{\text{PE}}$, which correspond to the structural difference coming from the fabrication error due to technological imperfections on each arm, the difference in modulation voltages applied to each arm, and the difference in the photoinduced index change between the two arms, respectively. The electro-optic phase $\Delta\theta_E$ can be expressed as

$$\Delta\theta_E = \pi \frac{\Delta V}{V_\pi}, \quad (5)$$

where V_π is the driving voltage required for the phase modulator to provide π phase, and $\Delta V = V_{\text{arm1}} - V_{\text{arm2}}$ refers to the modulated voltage difference between the two arms. We assume that $V_{\text{arm1}} = -V_{\text{arm2}} = V_{\text{app}}$ for electrode working at the push-pull mode.

The PE phase $\Delta\theta_{\text{PE}}$ is equal to $\theta_{\text{PE}}^1(I_{\text{ir}}^1) - \theta_{\text{PE}}^2(I_{\text{ir}}^2)$. Then we can calculate the total phase difference between two

arms as

$$\Delta\theta = \Delta\theta_0 + V_{\text{app}} \left[\frac{2\pi}{V_{\pi}} - \frac{C}{d} \Delta^+ f(I_{\text{ir}}) \right] + D \Delta^- f(I_{\text{ir}}). \quad (6)$$

This equation applies to any MZI-based LN devices and has been simplified by introducing $C = 2a\pi L_E/\kappa\lambda_0$ and $D = 2\pi L/\lambda_0$, where a is a constant [18], λ_0 is the free-space wavelength of the signal laser, and L is the length of arm. We also define a function $f(I_{\text{ir}}^j) = A I_{\text{ir}}^j / (1 + B I_{\text{ir}}^j)$, which is the index change only depending on I_{ir} [18], where $A = n^3 r_{33} \gamma \kappa a / 2\sigma_d$ and $B = \alpha a / \sigma_d$. Because of the different PEs on each arm, we have

$$\Delta^{\pm} f(I_{\text{ir}}) = f(I_{\text{ir}}^1) \pm f(I_{\text{ir}}^2), \quad (7)$$

Therefore, when we use a MZI-based VOA to analyze the effect of IPA, the μ in Eq. (6) is the MPN of signal pulses after attenuation and we can see that it is affected by both I_{ir} and V_{app} . This enables Eve to control the attenuation and execute IPA.

III. EXPERIMENT

As shown in Fig. 2, we design experiments to verify the effect of IPA on VOA. A 1550-nm laser (laser 1) exports the signal pulses and 1% of its output is routed by the 1:99 beam splitter (C2) to the optical power meter A (PM A) to monitor its stability. The LN device we test is a commercial MZI-based VOA (iXblue MXAN-LN-10) and its temperature is kept stable at 30 °C within an accuracy of 0.01 °C by a temperature control module (TCM) to avoid the effect of temperature drift on our test. The attack module (see Appendix B for more details) is used to insert the channel and execute IPA. In this module, the irradiation laser (laser 2) is selected at 405 nm because LN has higher photorefractive sensitivity at a shorter wavelength [21] and its power is tunable from 0 to 20 mW. Here we achieve the inverse injection of the irradiation beam into VOA through a fiber 50:50 BS (C2). The optical power meter B (PM B) is employed to monitor the effect of IPA. Given that the irradiation beam causes a small response of PM B, a fiber circulator is used here to block the reflected irradiation beam and avoid its influence on our test because the circulator can isolate the irradiation beam very well (see Appendix D).

To analyze how IPA impacts QKD, the signal intensity change is represented by magnification M obtained by dividing the attacked signal intensity by the original ones and we test it for different irradiation powers [Fig. 3(a)]. Here we set the original state of VOA at its maximum attenuation (i.e., its minimum output I_0 at working voltage $V_0 = 5.8$ V) to demonstrate IPA more clearly. Under IPA, the VOA's attenuation decreases and this process corresponds to the change from the green point to the blue

one along the dotted line of V_0 in Fig. 3(b). As shown in Fig. 3(a), the index change gradually saturates as the injection duration increases and then we get saturated M . As we analyzed, both the saturated M and response speed increase at higher irradiation powers, which corresponds to increases in $\Delta n_s(I_{\text{ir}})$ and $1/\tau$, respectively.

In Fig. 3(a), the saturated M decreases slightly when the irradiation power is larger than 6.26 μ W. This essentially stems from the saturation property of PE, i.e., $\Delta n_s(I_{\text{ir}})$ also tends to saturation [18]. Since $I_{\text{ir}}^1 \neq I_{\text{ir}}^2$, with the increase in I_{ir} , the index change of the arm with higher irradiation power reaches saturation first while that in another arm still increases. This results in a decrease in phase difference between the two arms and, consequently, a decrease in the saturated M . We can see that the VOA's attenuation can even be impacted at only 3-nW irradiation power. We note that these powers are measured at the connection between the VOA and C2. Therefore, the irradiation power actually entering the LN waveguide is lower than what we measure considering the couple loss between the fiber and the LN chip inside the VOA package.

Considering more general cases, the VOA's output may not be the minimum value while some intermediate value [such as I_1 in Fig. 3(b)] is more common. In this case, there are two working states of VOA that can output I_1 , corresponding to working on the falling (V_A) and rising (V_B) edges of its voltage curve. Under IPA, the voltage curve of VOA shifts from the initial (green) line to the attacked (blue) one. Our attack is working (e.g., V_A) as long as the attacked voltage curve is above the initial one (the blue-shaded area). However, the working state of VOA is sometimes unsuitable for attacks. For example, the attenuation increases instead when the working voltage (e.g., V_B) is outside the blue-shaded area.

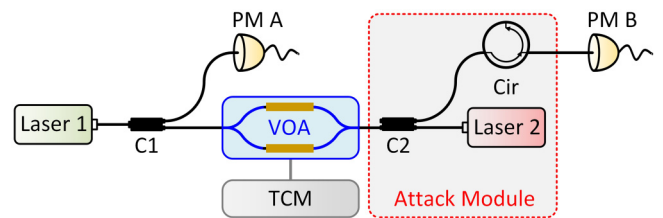


FIG. 2. Sketch of the experimental setup. Laser 1, a 1550-nm signal laser (Agilent 81960A). C1, coupler 1, a fiber 1:99 polarization-maintaining BS. PM A, power meter A (Dwin BD613C). VOA, schematic diagram of the internal structure of the variable optical attenuator (iXblue MXAN-LN-10). The blue lines and yellow blocks are LN waveguides and modulating electrodes, respectively. TCM, a temperature control module (Oeshine TCM-M207). C2, coupler 2, a fiber 50:50 BS. Cir, a fiber circulator. Laser 2, the 405-nm irradiation laser (Max-Ray FL-405-20-SM-B). PM B, power meter B (Thorlabs PM100D with S132C). Since the LN-based VOA is polarization dependent, the polarization-maintaining fibers are used here to connect laser 1, C1, and VOA.

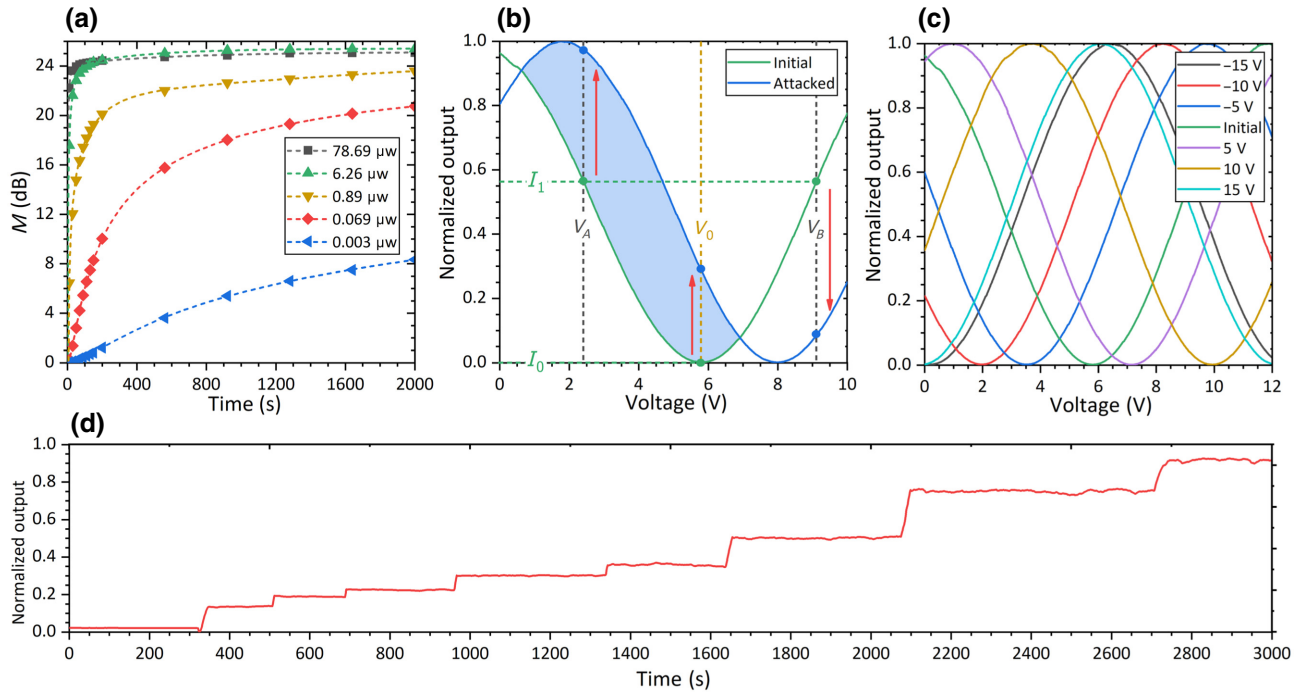


FIG. 3. (a) Variation of M obtained by dividing the attacked signal intensity by the original one is shown here in logarithmic coordinates on the y axis. (b) Schematic of IPA at different working voltages. (c) The result of the pretreatment technique with 12- μW irradiation power under different applied electric fields. (d) The result of the pulse-injection technique with 12- μW peak power and 10-s period pulses.

To make IPA available, the user-calibrated working voltage should be located in the blue area. In addition, since PE is voltage dependent [Eq. (2)], it is better to have a working voltage as high as possible to produce larger PE. These objectives can be achieved by the pretreatment technique. According to Eq. (2), we treat LN devices by injecting the irradiation beam until saturation under appropriate E_{app} and I_{ir} and then turn off the applied electric field and irradiation beam simultaneously. Considering the PE in LN always persists for several weeks or longer (in the absence of the applied electric field or any other treatments) [2], the pretreatment results can remain in LN devices long enough to affect their working states in QKD systems. As shown in Fig. 3(c), by using the irradiation laser at the continuous-wave mode and applying I_{ir} at 12 μW with different V_{app} , we can shift the static bias of the VOA's voltage curve to any position of the entire 2π range. Based on this technology, Eve can preset the original state of VOA to the most beneficial state for IPA before delivering it to users.

Furthermore, we propose the pulse-injection technique to enable fast, accurate, and arbitrary controllable attacks. This technique is performed by operating the irradiation laser at the pulse mode. In this technique, fast response (small τ) and significant index change [large $\Delta n_s(I_{\text{ir}})$] can be achieved by utilizing sufficiently high peak power

pulses, while arbitrary precision manipulation can be ensured by controlling the duty cycle and frequency of injected pulses. In our experiment, the peak power of injected pulses is 12 μW . To better demonstrate this technique, we use 10-s period pulses and deliberately perform multiple injections. During the injection, we use 1-s width pulses to change the output of VOA. When the desired extent of IPA is reached, we decrease the duty cycle of pulses to stabilize the effect of our attack, which is essentially to offset the decay behavior of PE [22].

As shown in Fig. 3(d), by finely tuning the duty cycle of pulses, the extent of IPA can be controlled at will and the effect of IPA can be well stabilized. To demonstrate the effect of pulse injection technology more clearly, the maximum attenuation state of VOA is processed to around 0 V through the pretreatment technique at -15-V applied electric field with 12- μW irradiation power. According to Fig. 3(c), the effect of IPA would be further enhanced if an applied electric field is present during this test. Therefore, to demonstrate only the effect of the irradiation beam itself, here we do not apply any external electric field; hence, the output of VOA cannot be modulated to its maximum attenuation state exactly and this is why the starting point of Fig. 3(d) is slightly deviated from the minimum value. In other words, under the current conditions, here we show only the lower limit of the effect for IPA. In practical attack

scenarios, faster and more accurate attacks can be achieved by programmed automatic feedback control of the irradiation laser. More details about the experiments are given in Appendix C.

IV. IPA AGAINST THE BB84 QKD

We use the decoy-state Bennett-Brassard 1984 (BB84) protocol [23] to analyze the security suffering from IPA (i.e., M). In our simulation, the overall transmittance of Bob's detection apparatus is 0.1, the fiber loss is 0.2 dB/km, the probability that a photon hit the erroneous detector is 0.5%, and the dark count rate is 6×10^{-7} . At the transmitter, Alice sends weak laser pulses with Poissonian photon-number distribution and the MPN of these signal pulses and decoy pulses are attenuated to μ and ν , respectively. The total transmittance between Alice and Bob is η , which can be regarded as the product of the transmission of the quantum channel $\eta_{AB} = 10^{-\alpha L/10}$ and η_B (the internal efficiency of Bob). When there is no eavesdropper, the MPN of signal pulses at Bob is $\eta\mu$ and still Poissonian. The response rate of the signal state at Bob is $Q_\mu = Y_0 + 1 - e^{-\eta\mu}$, where Y_0 is the dark count rate. Under the IPA, the attenuation of VOA is degraded so that the attacked MPN of the signal state is $\mu_e = M\mu$, namely, the MPN is amplified M times for both signal and decoy states. Then Eve intercepts all pulses from Alice and resends each photon to Bob with probability p . The remaining photons not sent to Bob are stored in quantum memory. Note that there is no need for Eve to be able to distinguish the photon number in each pulse. The probability of a successful attack can be defined as Eve storing and resending at least one photon that can be detected by Bob, that is,

$$p_s = \sum_{n=2}^{\infty} P_{\mu_e}(n) \sum_{m=1}^{n-1} C_n^m p^m (1-p)^{n-m} [1 - (1-\eta_B)^m]. \quad (8)$$

Eve's attack is always defined as a failure for pulses with only one photon, even if it has a probability of $1-p$ of being intercepted. This attack causes the photon-number distribution to change to

$$\begin{aligned} P_{\text{att}}(n) &= \sum_{m=n}^{\infty} P_{\mu_e}(m) (1-p)^m \left(\frac{p}{1-p}\right)^n C_m^n \\ &= e^{-Mp\mu} \frac{(Mp\mu)^n}{n!}, \end{aligned} \quad (9)$$

which is still Poissonian distribution and the MPN is $Mp\mu$. At the internal efficiency of Bob, η_B , the response rate of pulses with n photons is $Y_n^{\text{att}} = Y_0 + 1 - (1-\eta_B)^n (n \geq 1)$. Then the response rate of the signal state after being

attacked can be detected as

$$Q'_\mu = \sum_{n=1}^{\infty} P_{\text{att}}(n) Y_n^{\text{att}} = Y_0 + 1 - e^{-M\mu p \eta_B}. \quad (10)$$

To avoid disturbing the count rate of signal states detected by Bob, Eve should keep $Q'_\mu = Q_\mu$, that is,

$$p = \frac{\eta_{AB}}{M}. \quad (11)$$

For decoy-state pulses, we can get the same results for $Q'_\nu = Q_\nu$. In other words, if Eve intercepts all pulses and resends each photon to Bob with probability $p = \eta_{AB}/M$, she will not be detected through monitoring the count rate of the signal and decoy states. After the public discussion part of the QKD protocol, Eve can get the same result as Bob by measuring the stored signal photons on the same basis.

Because of the undisturbed response rate on the signal and decoy states, the tagged bit rate estimated by legal users is [24]

$$\Delta = \frac{Q_\mu - P_0 Y_0 - P_1 Y_1}{Q_\mu} \approx 1 - \frac{P_1 Y_1}{Q_\mu}, \quad (12)$$

where Y_1 is the lower bound of the single-photon yield, Q_μ is the response rate of signal state pulses with MPN μ , and P_i , $i \in \{0, 1\}$, is the i -photon probability of the Poissonian distribution pulses. However, the actual Δ is affected by IPA, that is,

$$\Delta^{\text{att}} = \sum_{n=2}^{\infty} \frac{P_{\mu_e}(n)}{Q_\mu} \sum_{m=1}^{n-1} C_n^m p^m (1-p)^{n-m} [1 - (1-\eta_B)^m], \quad (13)$$

where μ_e is the MPN of signal states suffering from IPA, expressed as $\mu_e = M\mu$, and η_B is the internal efficiency of Bob. The secret key per pulse is calculated as [25]

$$R = Q_\mu \{ (1 - \Delta^{\text{att}}) [1 - H_2(e_1)] - f H_2(E_\mu) \}, \quad (14)$$

where $H(x) = -x \log_2 x - (1-x) \log_2 (1-x)$ is Shannon's binary entropy function, e_1 is the upper bound of the single-photon quantum bit error rate (QBER) estimated by the decoy-state method, $f = 1.16$ is the error-correction efficiency, and E_μ is the overall signal state QBER. The attack does not change the counting rate of the signal and decoy states, and both e_1 and E_μ are identical to a no-attack event, which means that Eve can partially or even completely steal the security key without being discovered by users.

As shown in Fig. 4, the key measured by users is estimated based on the actual response rate of detectors, but

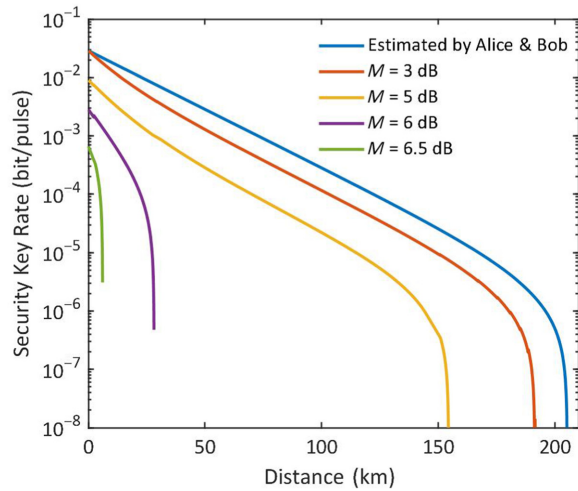


FIG. 4. The secret key rate under different M (decibels). The blue line is the key rate estimated by Alice and Bob based on their measurement results.

the actual secure key is much smaller because of the underestimated Δ . When M reaches 6.5 dB, there is no security key anymore, which means that the security can be totally broken by even the weakest irradiation power in our experiment, that is, the irradiated power of 3-nW in Fig. 3(a), corresponding to $M \approx 8.3$ dB. Such a weak injection light not only reduces the requirements of C2 but also makes it more difficult to detect the existence of IPA.

V. DISCUSSION

To counter IPA, filters such as dense wavelength division multiplexing modules may be insufficient because some channels do not have enough attenuation of irradiation beams (see Appendix D). Additionally, the optical power meters without a small enough power range are insufficient to detect an irradiation power as small as 3 nW. Fortunately, we find that the commonly used isolator and circulator have a huge attenuation of irradiation beams (see Appendix D); thus, they are necessary to isolate the injected beam from channels. However, the security of isolators and circulators also needs further study because they may be affected by the laser-damage attack [7,26] and external magnetic fields [27]. Since PE is fabrication dependent [18], defect engineering may be useful to reduce PE by doping with various impurities [28].

In fiber systems, although we can substitute the LN-based VOA with other types [7], the remaining high-speed modulators made of LN are unavoidable [29,30]. Therefore, state monitoring of LN devices is necessary and bias control or stabilization techniques [31,32] for MZ modulators also help to counteract the effects of IPA. Interestingly, our research also reveals some countermeasures to resist IPA. For example, users can process the LN device to a controlled state by the pretreatment technique, and then use

the device at a state that unfavorable to IPA (such as V_B in Fig. 3(b)). For the LNOI platform, the tighter optical confinement and higher crystal defect concentration contribute to stronger PE [10]. Besides, recent research suggests some different properties of PE in LNOI [10,33], such as the faster response speed and minor optical mode distortion. Thus, more comprehensive considerations on fabrication processes and structural design are necessary to mitigate PE [28,34] in future LNOI-based integrated QKD research.

In conclusion, we reveal PE is a new mechanism that can cause loopholes in practical QKD systems. To confirm its threat to QKD, we propose two effective techniques to enable controllable attack and proceed to execute powerful hacking on a commercial VOA. Our experimental and security analysis results show that even the weakest irradiation power (3 nW) is sufficient to cause totally broken security. Considering that PE can be induced over a wide range of wavelengths (from ultraviolet to even 1549 nm [16]), more types of loopholes derived from PE may be caused and further investigation is needed. Given the importance of LN devices in QKD systems, PE-related security issues deserve more attention. Our work contributes to the development of practical security in QKD systems and opens a window to designing more secure integrated QKD systems in the future.

ACKNOWLEDGMENTS

We would like to acknowledge Professor Changling Zou for his valuable discussions. This work was partially carried out at the USTC Center for Micro and Nanoscale Research and Fabrication. This work is supported by the National Key Research and Development Program of China (2018YFA0306400); the National Natural Science Foundation of China (Grants No. 61622506, No. 61575183, No. 61627820, No. 61475148, No. 62105318, No. 61822115, and No. 61675189); the China Postdoctoral Science Foundation (2021M693098); and the Anhui Initiative in Quantum Information Technologies.

APPENDIX A: MORE DETAILS ABOUT THE PHOTOREFRACTIVE EFFECT

In the LN waveguide, under the illumination of an irradiation power I_{ir} , the space-charge field caused by the inhomogeneous charge distribution is [18–20]

$$E_s(I_{ir}, t) = \left[\frac{\kappa\alpha}{\sigma_d + \sigma_{ph}} I_{ir} - E_s(I_{ir}, 0) \right] (1 - e^{-t/\tau}) + E_s(I_{ir}, 0), \quad (\text{A1})$$

where α is the absorption coefficient of the donor or acceptor centers; σ_d and σ_{ph} are the dark conductivity and photoconductivity, respectively; and κ is the Glass constant, which is related to the size of the waveguide. The

value of I_{ir} here is the average spatial intensity of the irradiation beam passing through the waveguide cross section, and τ is the build-up time constant of the space-charge field. This space-charge field influences the signal beam by modulating the index of the waveguide through the linear electro-optic effect

$$\begin{aligned}\Delta n(I_{\text{ir}}, t) &= \frac{n^3 r_{33} \gamma}{2} E_s(I_{\text{ir}}, t) \\ &= \Delta n_s(I_{\text{ir}})(1 - e^{-t/\tau}),\end{aligned}\quad (\text{A2})$$

where n is the waveguide refractive index, r_{33} is the linear electro-optic coefficient, and γ is the overlap integral of the optical mode profile and the space-charge field. This is the time response characteristic of PE, that is, the photorefractive index change saturates with increasing irradiation time due to the time response function of type $1 - e^{-t/\tau}$.

Because of the outstanding electro-optical modulation characteristics, the LN waveguide usually works in the presence of an external electric field, which interacts with the photogenerated charges and also affects E_s . Since the build-up time constant τ is of the order of 10^3 s for both Ti-in-diffusion and the proton-exchanged LN waveguide [35], the influence of high-speed radio-frequency signals on photogenerated carriers is averaged out and only leaves its direct current component, which can be written as an external static electric field E_{app} . Therefore, the saturated photorefractive index change $\Delta n_s(I_{\text{ir}})$ should be

$$\begin{aligned}\Delta n_s(I_{\text{ir}}) &= \frac{n^3 r_{33} \gamma}{2} E_s(I_{\text{ir}}, t) \Big|_{t \rightarrow \infty} \\ &= \frac{n^3 r_{33} \gamma}{2} \left(-\frac{\sigma_{\text{ph}}}{\sigma} E_{\text{app}} + \frac{\kappa \alpha}{\sigma} I_{\text{ir}} \right),\end{aligned}\quad (\text{A3})$$

where $\sigma = \sigma_d + \sigma_{\text{ph}}$.

When the irradiation intensity is low, for instance, lower than 100 W/cm^2 (or about $7 \mu\text{W}$) for the LN waveguide made by Ti-in-diffusion in Ref. [18], which assumes that the photoconductivity varies linearly with the irradiation intensity,

$$\sigma_{\text{ph}} = \alpha \alpha I_{\text{ir}}, \quad (\text{A4})$$

where $a = e\mu\tau_0\phi/h\nu$ is a constant, which is related to the electronic charge e , the photon energy $h\nu$, the electron mobility μ , the quantum efficiency ϕ , and the carrier lifetime τ_0 . Then we can obtain the saturated phase change of the LN waveguide as

$$\begin{aligned}\theta_{\text{PE}}(I_{\text{ir}}) &= \frac{2\pi}{\lambda_0} \left(-\frac{a}{\kappa} L E_{\text{app}} + L \right) f(I_{\text{ir}}) \\ &= (-CE_{\text{app}} + D)f(I_{\text{ir}}).\end{aligned}\quad (\text{A5})$$

Here we introduce $C = 2a\pi L E_{\text{app}}/\kappa\lambda_0$ and $D = 2\pi L/\lambda_0$, where λ_0 is the free-space wavelength, L is the arm length

of a MZI, and L_E is the length of the waveguide modulated by the electric field. In this equation, $f(I_{\text{ir}})$ is the saturated photoinduced refractive index change related to only the irradiation intensity [18]:

$$f(I_{\text{ir}}) = \frac{A I_{\text{ir}}}{1 + B I_{\text{ir}}} \quad (\text{A6})$$

with $A = n^3 r_{33} \gamma \kappa a / 2 \sigma_d$ and $B = \alpha \alpha / \sigma_d$. We can see that the change in the photoinduced phase is related to both the applied electric field and the irradiation beam.

At high irradiation intensity (as before, larger than 100 W/cm^2 for the Ti-in-diffusion waveguide), the photoconductivity can be conveniently assumed to be proportional to $(I_{\text{ir}})^{1/m}$, where m is an integer greater than 1 [36]. Because of the very large I_{ir} , we have $\sigma_{\text{ph}} \gg \sigma_d$, and

$$f(I_{\text{ir}}) = \frac{A}{B} (I_{\text{ir}})^{1-1/m}. \quad (\text{A7})$$

Then Eq. (A5) should be rewritten as

$$\theta_{\text{PE}}(I_{\text{ir}}) = -\frac{A}{B} C E_{\text{app}} + D f(I_{\text{ir}}). \quad (\text{A8})$$

From both Eqs. (A6) and (A7), we can see that the saturated photoinduced refractive index change also tends to saturate with increasing the irradiation power. Therefore, PE does not become infinitely large with increasing I_{ir} . This is the saturation characteristic of PE.

In practical applications, researchers can dope different impurities to enhance or weaken PE in a LN crystal to make devices suitable for different application scenarios [37–39]. However, the doping techniques are not mature enough and increase costs, and have thus not been widely used in commercial devices.

In addition to doping, the photorefractive sensitivity depends on the specific fabrication procedure, including Ti-in-diffusion technology, proton exchange, annealed proton exchange (APE), reverse proton exchange (RPE), and soft proton exchange (SPE) [40]. In Eqs. (A5) and (A6), the contribution of dark conductivity to PE is dominant at a lower irradiation power. So the photorefractive sensitivity of devices fabricated by Ti-in-diffusion technology is higher than that of other processes because of lower dark conductivity. Benefitting from the increased dark conductivity induced by the proton exchange process, proton-exchanged waveguides exhibit the highest robustness to PE but are penalized by degradation of electro-optic and nonlinear optic properties. APE, RPE, and SPE can partially recover the degradation of material properties during fabrication, but are accompanied by an increase in photorefractive sensitivity [3, 18, 40]. At high irradiation power, the influence of PE can be characterized by Eqs. (A7) and (A8). This means that the saturated index change is independent of dark conductivity, so the photorefractive index

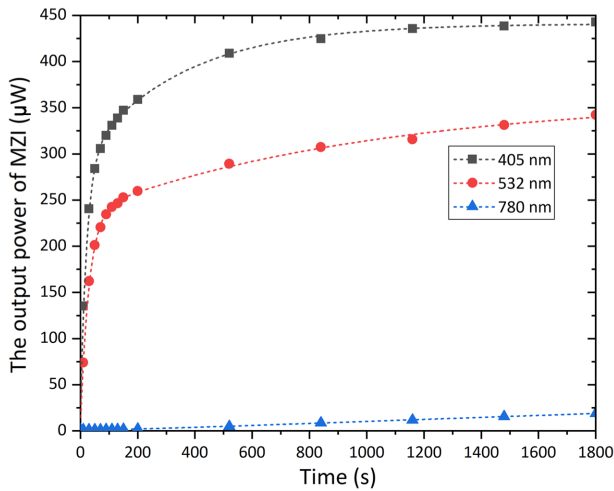


FIG. 5. The wavelength dependence of PE. The time response curve of VOA under irradiation beams at 405 nm (black), 532 nm (red), and 780 nm (blue), respectively. The y axis is the output power of VOA and the x axis is the injection duration. The VOA is initialized to the maximum attenuation before each test.

change in the LN waveguide at higher irradiation power is almost the same for all these fabrication procedures [22,35].

APPENDIX B: DESIGN OF THE ATTACK MODULE

The selection of irradiation wavelength depends on the photorefractive sensitivity of the LN material. Here we test the wavelength dependence of PE. To compare the effect of PE, the irradiation power is set to $16 \mu\text{W}$ for each wavelength and the results are shown in Fig. 5. The irradiation beam at 405 nm has the fastest response and most substantial effect. This phenomenon is consistent with the result of Fujiwara *et al.* [21,35] and due to LN having a higher photorefractive sensitivity at shorter wavelengths. Additionally, the PE-based attack works over a wide range of wavelengths (from ultraviolet to even 1549 nm [16,33], which is close to the commonly used communication wavelength). This increases the difficulty of defense because a band-pass filter with a sufficiently wide working wavelength range is needed to filter the irradiation beam. Therefore, our experiment uses an irradiation laser at 405 nm for a more efficient attack.

To couple the irradiation beam into the communication channel, the coupling efficiency of different commercially available fiber devices working at 1550 nm has been tested, including the circulator, 50:50 BS, 90:10 BS, and 99:1 BS. We find that the circulator isolates almost all irradiation power at 405 nm. We measure the BSRs of these fiber BSs and the transmission loss (TL) when used in the attack module at 405 and 1550 nm. Table I shows the measure result. The TL includes both insertion loss and splitting

TABLE I. The 1*2 BS is the fiber beam splitter with one input port and two output ports.

Type of BS	TL @1550 nm (dB)	BSR @405 nm	TL @405 nm (dB)
50:50 1*2 BS	3.4	88:12	7.41
90:10 1*2 BS	0.79	91:9	13.49
99:1 1*2 BS	0.41	92:8	15.5

loss. For an irradiation beam at 405 nm, in addition to insertion loss, about 90% of light passes through the bar port for all BSs. For the two unbalanced BSs, the bar port always has a larger splitting ratio. Therefore, we select the bar port to transmit the signal light to reduce the TL at 1550 nm. As a result, the TL at 405 nm for all unbalanced BSs is measured when the irradiation beam is coupled through the cross port. For the 50:50 BS, the TL of the two output ports is the same at 1550 nm, so we can transmit the attack beam through the bar port, and this is why the TL of the 50:50 BS is much lower than the other two BSs.

In an actual communication system, the channel loss caused by the eavesdropper should be as small as possible. The best strategy to inject the attack beam is using a MZI based on two 50:50 BSs. Both bar ports of BSs are used to transmit the irradiation beam, and both the cross ports are used to pass the signal light. A schematic diagram of this method is shown in Fig. 6. The phase difference in a MZI is modulated to π by the phase modulator to make the signal beam output through the cross port. The TL of a MZI at 405 nm that we measure is about -8.31 dB , which is still lower than the other two unbalanced BSs. Theoretically, the TL at 1550 nm for this scheme is negligible. In our experiment, for the sake of simplicity, the attack beam is reversely fed into the MZI by a 50:50 BS. It is worth noting that this does not affect the main conclusions of this article.

APPENDIX C: EXPERIMENTAL METHOD

To ensure the consistency of our experiments, the comparison of PE between different powers or wavelengths should be performed in the same state of VOA. However, as shown in Fig. 7, the static bias of VOA is changed after each injection. Hence, it is essential to recover the state of VOA to the same initial state before each experiment. The

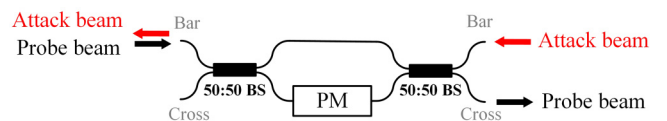


FIG. 6. MZI-based scheme includes two 50:50 BSs and a phase modulator (PM). Almost all attack power goes through the bar path of each BS. The phase modulator is used to interfere all signal power into the cross port of a MZI.

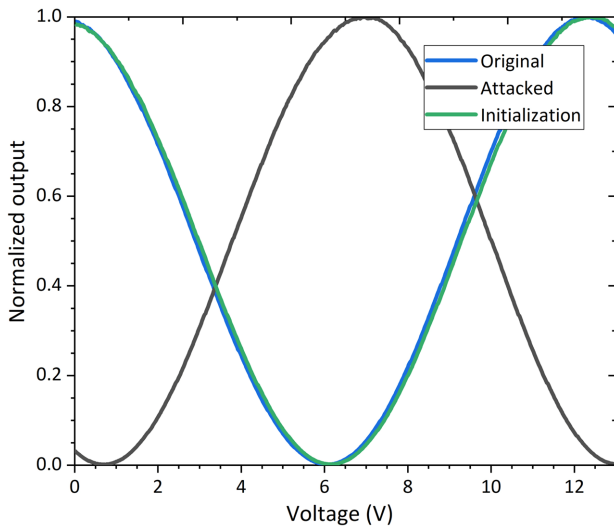


FIG. 7. Initialization of VOA. The VOA’s original and attacked voltage curves are shown as the blue and black lines, respectively. Using the initialization method, the voltage curve can be initialized to the green line, which is almost the same as the original one.

recovery of the carrier distribution depends on the dark conductivity [41] of LN and usually persists for a long time [2]. Treating samples by heating, annealing, or uniform illuminating with a high-intensity halogen bulb can accelerate this process [3,42]. Essentially, these methods erase the space-charge distribution (restoring the LN material to the state before injection) by enhancing the charge mobility. But here, since the commercial device is already packaged, we cannot use these initialization methods.

Fortunately, although the space-charge distribution cannot be erased, it can be redistributed to the same state before each experiment based on our pretreatment technique. Here, we initialize our VOA by injecting the irradiation beam at $4.39 \mu\text{W}$ until saturation under a 0-V external electric field. As we expected, the green line in Fig. 7, the result of initializing, is almost the same as the original one. All of our tests are initialized with this method.

APPENDIX D: LOSS OF THE IRRADIATION BEAM IN DEVICES WORKING AT 1550 nm

To explore countermeasures against IPA, we measure the loss of the irradiation beam in some commonly used devices in QKD systems. Table II lists the TLs of these three irradiation wavelengths in a single-mode fiber in compliance with the ITU-T G.652.D and the insertion losses of the isolator, circulator, and some channels of the dense wavelength division multiplexing (DWDM) module. Considering the nanowatt magnitude irradiation power, we think that the TL is acceptable because Eve can attack at 1 km (which is an available distance) from the

TABLE II. TLs of irradiation beams in a single-mode fiber and insertion losses of the isolator, circulator, and dense wavelength division multiplexing (DWDM) module working at 1550 nm. For DWDM aligned on the ITU grid, channels 33 (C33) and 35 (C35) are aligned to 1550.92 and 1549.32 nm, respectively.

Wavelength (nm)	TL (dB/km)	DWDM		Isolator (dB)	Circulator (dB)
		C33 (dB)	C35 (dB)		
405	13	33	61	> 78	> 78
532	14	71	> 78	> 78	> 78
780	3	15	31	58	73

users. Moreover, QKD systems always output with narrowband optical filters such as DWDM aligned on the ITU grid. But we find that the loss of the irradiation beam at 405 and 780 nm is also acceptable. For example, the total loss is 46 dB at 405 nm when a QKD system output at 1550.92 nm and Eve attacks at 1 km. It requires $120\text{-}\mu\text{W}$ irradiation power and this is easily available.

Learning from the Trojan-horse attack [43,44], the commonly used defenders such as the isolator and circulator are necessary to isolate the injected beam. Fortunately, they have very large transmittance losses at the irradiation wavelengths we use. Take the 405-nm irradiation beam as an example; the total loss is larger than 90 dB when Eve attacks at 1 km from the users regardless of whether the isolator or circulator is used. This means that even considering the weakest case (3 nW in our experiment), the power required by Eve already reaches the watt magnitude. To defend the Trojan-horse attack, the required isolation in different QKD systems is usually greater than 100 dB [43,44], which corresponds to at least three of the isolators we tested here (36 dB for each at 1550 nm). This contributes to a huge attenuation and makes the injection of

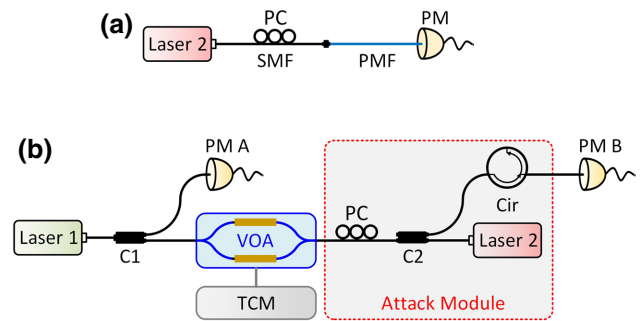


FIG. 8. Sketches of the experimental setup. PC, polarization controller. SMF, single-mode fiber, which is the black line. PMF, polarization-maintaining fiber, which is the blue line. The remaining devices are the same as in Fig. 2 in the main text. (a) Polarization-dependent loss test of the irradiation beam passing through the polarization-maintaining fiber. (b) Polarization dependence test of the irradiation beam on PE.

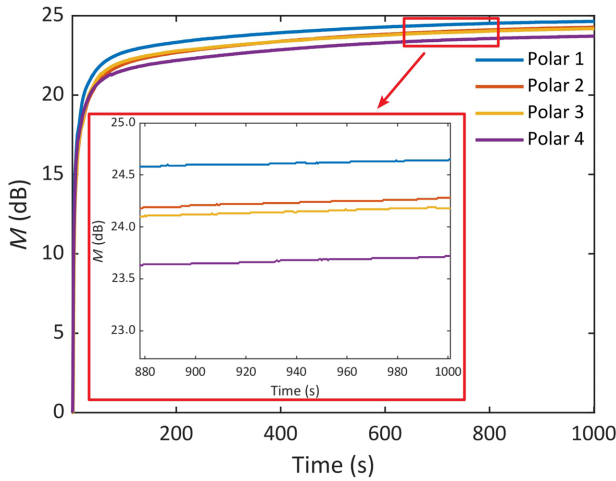


FIG. 9. Change in the VOA’s output at different irradiation polarizations. The blue (polar 1) and purple (polar 4) lines correspond to the polarization of the irradiation beam that has maximum and minimum transmittance through the PMF, respectively. The red (polar 2) and yellow (polar 3) lines are the other two polarization states that are different from the blue and purple ones.

irradiation beams almost impossible. However, the security of isolators and circulators can also be affected by the laser-damage attack and thus further research is still necessary [7,26].

APPENDIX E: IMPACT OF OTHER DIMENSIONS ON IPA

In addition to the irradiation power, the applied electric field, and the injection duration, we further investigate the effect of the polarization and wavelength of the irradiation beam on IPA.

The mechanism of how the irradiation polarization affects PE is complex [45] and may include various factors such as the change of coupling efficiency of the irradiation beam and the absorption process of irradiation photons. Therefore, further in-depth analysis is needed in our future research. Here, to learn how much the effect of polarization on M is, we investigate it experimentally.

We first test the polarization-dependent loss (PDL) of the irradiation beam passing through a polarization-maintaining fiber (PMF). Since the output fiber of the VOA is a PMF, we should know the PDL of the irradiation beam in PMF to deduce the change in the irradiation power in the VOA. As shown in Fig. 8(a), the irradiation beam’s polarization is modulated by a polarization controller (PC) and then fed into a PMF. The transmittance is recorded by the optical power meter (PM) while randomly adjusting the PC. According to our test, the PDL is just about 0.1 dB, that is, the polarization of the irradiation beam does not affect the irradiation power fed into the VOA. Then we test

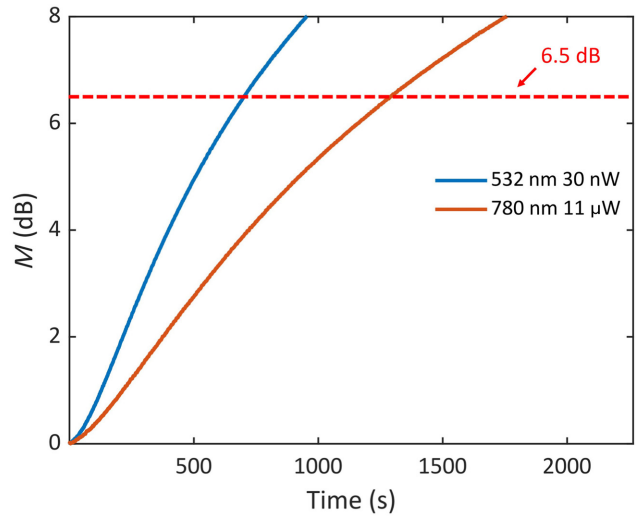


FIG. 10. Effect of the irradiation beam at 532 and 780 nm.

the effect of the irradiation beam at different polarizations using the PC to control its polarization. The experimental setup is shown in Fig. 8(b) and the results are given in Fig. 9. We modulate four different polarization states: “polar 1” and “polar 4” correspond to the polarization state that has the maximum (about -18.78 dBm) and minimum (about -18.92 dBm) irradiation power across the PMF, respectively; “polar 2” and “polar 3” are the other two different polarization states. As the results show, there is only a 0.93-dB effect on M for different polarization states and it is almost negligible for IPA.

The attack effect of different irradiation wavelengths at the same power is shown in Fig. 5; here we investigate the power required for a successful attack at each wavelength. As shown in Fig. 10, the dotted line represents the magnification ($M = 6.5$ dB according to the security analysis in Fig. 4) required to steal the security key completely and this can be achieved by both the 30-nW 532-nm irradiation beam and the 11- μ W 780-nm irradiation beam. However, there is no observable phenomenon for irradiation beams at 1550 nm, even at a power of up to 4 mW. Higher power is temporarily unavailable in our apparatus, but we will investigate the relevant issues in forthcoming work. Here, we can gain relevant knowledge from the work of Kostritskii [16], that is, the required power is larger than 100 mW for wavelengths near 1.5 μ m. This value can only be used as a reference since PE is dependent on both the fabrication process and the structure of the LN device.

[1] T. J. Hall, R. Jaura, L. M. Connors, and P. D. Foote, The photorefractive effect—a review, *Prog. Quantum Electron.* **10**, 77 (1985).
 [2] A. M. Glass, The photorefractive effect, *Opt. Eng.* **17**, 175470 (1978).

- [3] F. Mondain, F. Brunel, X. Hua, E. Gouzien, A. Zavatta, T. Lunghi, F. Doutré, M. P. De Micheli, S. Tanzilli, and V. D'Auria, Photorefractive effect in LiNbO₃-based integrated-optical circuits for continuous variable experiments, *Opt. Express* **28**, 23176 (2020).
- [4] G. T. Harvey, The photorefractive effect in directional coupler and Mach-Zehnder LiNbO₃/sub 3/ optical modulators at a wavelength of 1.3 μm , *J. Lightwave Technol.* **6**, 872 (1988).
- [5] Ken-ichiro Yoshino, Mikio Fujiwara, Kensuke Nakata, Tatsuya Sumiya, Toshihiko Sasaki, Masahiro Takeoka, Masahide Sasaki, Akio Tajima, Masato Koashi, and Akihisa Tomita, Quantum key distribution with an efficient countermeasure against correlated intensity fluctuations in optical pulses, *Npj Quantum Inf.* **4**, 8 (2018).
- [6] Kejin Wei, Weijun Zhang, Yan-Lin Tang, Lixing You, and Feihu Xu, Implementation security of quantum key distribution due to polarization-dependent efficiency mismatch, *Phys. Rev. A* **100**, 022325 (2019).
- [7] Anqi Huang, Ruoping Li, Vladimir Egorov, Serguei Tchouragoulov, Krtin Kumar, and Vadim Makarov, Laser-Damage Attack Against Optical Attenuators in Quantum Key Distribution, *Phys. Rev. Appl.* **13**, 034017 (2020).
- [8] Andreas Boes, Bill Corcoran, Lin Chang, John Bowers, and Arnan Mitchell, Status and potential of lithium niobate on insulator (LNOI) for photonic integrated circuits, *Laser Photon. Rev.* **12**, 1700256 (2018).
- [9] Jintian Lin, Fang Bo, Ya Cheng, and Jingjun Xu, Advances in on-chip photonic devices based on lithium niobate on insulator, *Photonics Res.* **8**, 1910 (2020).
- [10] Di Zhu, Linbo Shao, Mengjie Yu, Rebecca Cheng, Boris Desiatov, C. J. Xin, Yaowen Hu, Jeffrey Holzgrafe, Soumya Ghosh, Amirhassan Shams-Ansari, Eric Puma, Neil Sinclair, Christian Reimer, Mian Zhang, and Marko Lončar, Integrated photonics on thin-film lithium niobate, *Adv. Opt. Photonics* **13**, 242 (2021).
- [11] Yu Xue, Ranfeng Gan, Kaixuan Chen, Gengxin Chen, Ziliang Ruan, Junwei Zhang, Jie Liu, Daoxin Dai, Changjian Guo, and Liu Liu, Breaking the bandwidth limit of a high-quality-factor ring modulator based on thin-film lithium niobate, *Optica* **9**, 1131 (2022).
- [12] Cheng Wang, Mian Zhang, Xi Chen, Maxime Bertrand, Amirhassan Shams-Ansari, Sethumadhavan Chandrasekhar, Peter Winzer, and Marko Lončar, Integrated lithium niobate electro-optic modulators operating at CMOS-compatible voltages, *Nature* **562**, 101 (2018).
- [13] Chunfeng Huang, Ye Chen, Long Jin, Minming Geng, Junwei Wang, Zhenrong Zhang, and Kejin Wei, Experimental secure quantum key distribution in the presence of polarization-dependent loss, *Phys. Rev. A* **105**, 012421 (2022).
- [14] Peng Ye, Wei Chen, Ze-Hao Wang, Guo-Wei Zhang, Yu-Yang Ding, Guan-Zhong Huang, Zhen-Qiang Yin, Shuang Wang, De-Yong He, Wen Liu, Guang-Can Guo, and Zheng-Fu Han, Transmittance-invariant phase modulator for chip-based quantum key distribution, *Opt. Express* **30**, 39911 (2022).
- [15] Ke Liu, Chen Ran Ye, Sikandar Khan, and Volker J. Sorger, Review and perspective on ultrafast wavelength-size electro-optic modulators: Review and perspective on ultrafast wavelength-size electro-optic modulators, *Laser Photon. Rev.* **9**, 172 (2015).
- [16] S. M. Kostritskii, Photorefractive effect in LiNbO₃-based integrated-optical circuits at wavelengths of third telecom window, *Appl. Phys. B* **95**, 421 (2009).
- [17] N. V. Kukhtarev, V. B. Markov, S. G. Odulov, M. S. Soskin, and V. L. Vinetskii, Holographic storage in electrooptic crystals. I. Steady state, *Ferroelectrics* **22**, 949 (1978).
- [18] Takumi Fujiwara, Ramakant Srivastava, Xiaofan Cao, and Ramu V. Ramaswamy, Comparison of photorefractive index change in proton-exchanged and Ti-diffused LiNbO₃ waveguides, *Opt. Lett.* **18**, 346 (1993).
- [19] R. A. Becker and R. C. Williamson, Photorefractive effects in LiNbO₃ channel waveguides: Model and experimental verification, *Appl. Phys. Lett.* **47**, 1024 (1985).
- [20] M. M. Howerton and W. K. Burns, Photorefractive effects in proton exchanged LiTaO₃/sub 3/ optical waveguides, *J. Lightwave Technol.* **10**, 142 (Feb./1992).
- [21] T. Fujiwara, S. Sato, and H. Mori, Wavelength dependence of photorefractive effect in Ti-indiffused LiNbO₃ waveguides, *Appl. Phys. Lett.* **54**, 975 (1989).
- [22] T. Fujiwara, H. Mori, and Y. Fujii, Evolution and decay behavior of the photorefractive effect in Ti : LiNbO₃ optical waveguides, *Ferroelectrics* **95**, 133 (1989).
- [23] Xiongfeng Ma, Bing Qi, Yi Zhao, and Hoi-Kwong Lo, Practical decoy state for quantum key distribution, *Phys. Rev. A* **72**, 012326 (2005).
- [24] D. Gottesman, Hoi-Kwong Lo, N. Lutkenhaus, and J. Preskill, in *International Symposium on Information Theory, 2004. ISIT 2004. Proceedings.* (IEEE, Chicago, Illinois, USA, 2004), p. 135.
- [25] Xiang-Bin Wang, Beating the Photon-Number-Splitting Attack in Practical Quantum Cryptography, *Phys. Rev. Lett.* **94**, 230503 (2005).
- [26] Anastasiya Ponosova, Daria Ruzhitskaya, Poompong Chaiwongkhot, Vladimir Egorov, Vadim Makarov, and Anqi Huang, Protecting Fiber-Optic Quantum Key Distribution Sources Against Light-Injection Attacks, *PRX Quantum* **3**, 040307 (2022).
- [27] Hao Tan, Wei-Yang Zhang, Likang Zhang, Wei Li, Sheng-Kai Liao, and Feihu Xu, External magnetic effect for the security of practical quantum key distribution, *Quantum Sci. Technol.* **7**, 045008 (2022).
- [28] Yongfa Kong, Fang Bo, Weiwei Wang, Dahuai Zheng, Hongde Liu, Guoquan Zhang, Romano Rupp, and Jingjun Xu, Recent progress in lithium niobate: Optical damage, defect simulation, and on-chip devices, *Adv. Mater.* **32**, 1806452 (2020).
- [29] M. Lucamarini, Z. L. Yuan, J. F. Dynes, and A. J. Shields, Overcoming the rate–distance limit of quantum key distribution without quantum repeaters, *Nature* **557**, 400 (2018).
- [30] Shuang Wang, Zhen-Qiang Yin, De-Yong He, Wei Chen, Rui-Qiang Wang, Peng Ye, Yao Zhou, Guan-Jie Fan-Yuan, Fang-Xiang Wang, Wei Chen, Yong-Gang Zhu, Pavel V. Morozov, Alexander V. Divochiy, Zheng Zhou, Guang-Can Guo, and Zheng-Fu Han, Twin-field quantum key distribution over 830-km fibre, *Nat. Photonics* **16**, 154 (2022).

- [31] Chang-Hoon Park, Min-Ki Woo, Byung-Kwon Park, Seung-Woo Jeon, Hojoong Jung, Sangin Kim, and Sang-Wook Han, Experimental demonstration of an efficient Mach-Zehnder modulator bias control for quantum key distribution systems, *Electronics* **11**, 2207 (2022).
- [32] George Iskander, N. Sinclair, C. Pena, S. Xie, and M. Spiropulu, Stabilization of an electro-optic modulator for quantum communication using a low-cost microcontroller, *Caltech Undergraduate Res. J.* **20** (2019).
- [33] Haowei Jiang, Rui Luo, Hanxiao Liang, Xianfeng Chen, Yuping Chen, and Qiang Lin, Fast response of photorefraction in lithium niobate microresonators, *Opt. Lett.* **42**, 3267 (2017).
- [34] Yuntao Xu, Mohan Shen, Juanjuan Lu, Joshua B. Surya, Ayed Al Sayem, and Hong X. Tang, Mitigating photorefractive effect in thin-film lithium niobate microring resonators, *Opt. Express* **29**, 5497 (2021).
- [35] Takumi Fujiwara, Xiaofan Cao, Ramakant Srivastava, and Ramu V. Ramaswamy, Photorefractive effect in annealed proton-exchanged LiNbO₃ waveguides, *Appl. Phys. Lett.* **61**, 743 (1992).
- [36] Elaine E. Robertson, Robert W. Eason, Yoshiatsu Yokoo, and Peter J. Chandler, Photorefractive damage removal in annealed-proton-exchanged LiNbO₃ channel waveguides, *Appl. Phys. Lett.* **70**, 2094 (1997).
- [37] D. A. Bryan, Robert Gerson, and H. E. Tomaschke, Increased optical damage resistance in lithium niobate, *Appl. Phys. Lett.* **44**, 847 (1984).
- [38] Milutin Stepić, Eugene Smirnov, Christian E. Rüter, Liv Prönneke, Detlef Kip, and Vladimir Shandarov, Beam interactions in one-dimensional saturable waveguide arrays, *Phys. Rev. E* **74**, 046614 (2006).
- [39] Christian E. Rüter, Konstantinos G. Makris, Ramy El-Ganainy, Demetrios N. Christodoulides, Mordechai Segev, and Detlef Kip, Observation of parity-time symmetry in optics, *Nat. Phys.* **6**, 192 (2010).
- [40] Marco Bazzan and Cinzia Sada, Optical waveguides in lithium niobate: Recent developments and applications, *Appl. Phys. Rev.* **2**, 040603 (2015).
- [41] A. M. Glass, I. P. Kaminow, A. A. Ballman, and D. H. Olson, Absorption loss and photorefractive-index changes in Ti:LiNbO(3) crystals and waveguides, *Appl. Opt.* **19**, 276 (1980).
- [42] Luigi Moretti, Mario Iodice, Francesco G. Della Corte, and Ivo Rendina, Temperature dependence of the thermo-optic coefficient of lithium niobate, from 300 to 515 K in the visible and infrared regions, *J. Appl. Phys.* **98**, 036101 (2005).
- [43] Hao Tan, Wei Li, Likang Zhang, Kejin Wei, and Feihu Xu, Chip-Based Quantum Key Distribution Against Trojan-Horse Attack, *Phys. Rev. Appl.* **15**, 064038 (2021).
- [44] M. Lucamarini, I. Choi, M. B. Ward, J. F. Dynes, Z. L. Yuan, and A. J. Shields, Practical Security Bounds Against the Trojan-Horse Attack in Quantum Key Distribution, *Phys. Rev. X* **5**, 031030 (2015).
- [45] P. Günter and J.-P. Huignard, eds., *Photorefractive Materials and Their Applications 1: Basic Effects*, Springer Series in Optical Sciences No. 113 (Springer, New York, NY, 2006).